Webster, J.M., Ravelo, A.C., Grant, H.L.J., and the Expedition 389 Scientists
Proceedings of the International Ocean Discovery Program Volume 389
publications.iodp.org

Site M0096[1]

J.M. Webster, A.C. Ravelo, H.L.J. Grant, M. Rydzy, M. Stewart, N. Allison, R. Asami, B. Boston, J.C. Braga, L. Brenner, X. Chen, P. Chutcharavan, A. Dutton, T. Felis, N. Fukuyo, E. Gischler, S. Greve, A. Hagen, Y. Hamon, E. Hathorne, M. Humblet, S. Jorry, P. Khanna, E. Le Ber, H. McGregor, R. Mortlock, T. Nohl, D. Potts, A. Prohaska, N. Prouty, W. Renema, K.H. Rubin, H. Westphal, and Y. Yokoyama[2]

[1] Webster, J.M., Ravelo, A.C., Grant, H.L.J., Rydzy, M., Stewart, M., Allison, N., Asami, R., Boston, B., Braga, J.C., Brenner, L., Chen, X., Chutcharavan, P., Dutton, A., Felis, T., Fukuyo, N., Gischler, E., Greve, S., Hagen, A., Hamon, Y., Hathorne, E., Humblet, M., Jorry, S., Khanna, P., Le Ber, E., McGregor, H., Mortlock, R., Nohl, T., Potts, D., Prohaska, A., Prouty, N., Renema, W., Rubin, K.H., Westphal, H., and Yokoyama, Y., 2025. Site M0096. In Webster, J.M., Ravelo, A.C., Grant, H.L.J., and the Expedition 389 Scientists, Hawaiian Drowned Reefs. Proceedings of the International Ocean Discovery Program, 389: College Station, TX (International Ocean Discovery Program). https://doi.org/10.14379/iodp.proc.389.103.2025

[2] **Expedition 389 Scientists' affiliations.**

Contents

Keywords
International Ocean Discovery Program, IODP, Expedition 389, *MMA Valour*, Hawaiian Drowned Reefs, Earth climate system, Earth system feedbacks, Earth history tipping points, Site M0096, coral reef, volcanics, sea level, paleoclimate, central Pacific, reef health, Hawaiian geology, basalt, lava, carbonates, Kawaihae

Core descriptions

Supplementary material

References (RIS)

MS 389-103
Published 26 February 2025

Funded by ECORD, JAMSTEC, and NSF OCE1326927

1. Operations

The multipurpose vessel *MMA Valour* was used as the drilling platform throughout Expedition 389. At all sites, dynamic positioning was used to provide accurate positions throughout operations and water depth was established using a Sound Velocity Profiler (SVP) placed on the top of the PROD5 drilling system. For more detail on acquisition methods, see **Introduction** in the Expedition 389 methods chapter (Webster et al., 2025).

Summary operational information for Holes M0096A–M0096F is provided in Table **T1**. All times stated are in Hawaiian Standard Time (HST).

1.1. Hole M0096A

The *MMA Valour* arrived at Site M0096 at 2324 h on 4 September 2023. Predeployment preparation was undertaken from 0000 to 0255 h on 5 September, and PROD5 was deployed at 0255 h to a water depth of 740.8 m. Recovery of PROD5 was initiated at 0700 h due to movement of the port tool magazine, and it was recovered to deck at 0940 h; no borehole was initiated. From 0940 to 1430 h, PROD5 was prepared for a second deployment at Site M0096, and it was deployed again at 1250 h. Coring operations in Hole M0096A were carried out from 1430 to 1815 h, when the bore-

Table T1. Hole summary, Site M0096. R = rotary coring mode, W = wash down mode. LAT = Lowest Astronomical Tide. **Download table in CSV format.**

Hole	Water depth (m)	Date started (2023)	Date finished (2023)	Latitude	Longitude	Coring method	Total drilled depth (m)	Recovered length (m)	Core recovery (%)	Cores (*N*)	Notes
389-											
M0096A	740.8	5 Sep	5 Sep	20.036388°	–156.065720°	R	1.78	1.62	91.11	2	LAT water depth: 740.2 m. Borehole abandoned due to technical issues.
M0096B	739.1	6 Sep	6 Sep	20.036439°	–156.065665°	W	0.99	0	0	1	LAT water depth: 738.5 m. Wash only to 0.99 m. No recovery. Borehole abandoned due to technical issues.
M0096C	739.9	6 Sep	6 Sep	20.036423°	–156.065688°	R, W	1.74	0.45	52.33	1	LAT water depth: 739.4 m. Washed down to 0.88 m. Cored 1.74–1.84 m. Rotary from 1.84 m couldn't penetrate. Borehole abandoned due to technical issues.
M0096D	736.8	7 Sep	7 Sep	20.036843°	–156.065610°	R	7.40	2.24	30.27	4	LAT water depth: 736.2 m. Borehole abandoned due to technical issues.
M0096E	738.2	19 Sep	19 Sep	20.036980°	–156.065609°	W	6.70	0	0	1	LAT water depth: 737.6 m. Wash only to 6.70 m. Borehole abandoned due to technical issues.
M0096F	738.2	20 Sep	20 Sep	20.036960°	–156.065596°	W, R	12.24	4.76	86.23	5	LAT water depth: 737.6 m. Washed to 6.72 m. Borehole abandoned due to technical issues.

hole had to be abandoned due to a mechanical issue with PROD5 (magazine wobble). PROD5 was recovered to deck at 1945 h on 5 September. Deck operations commenced, core barrels were extracted for curation, and mechanical adjustments were made.

Two cores were recovered from Hole M0096A from 1.78 m of rotary coring, and the total recovered core length was 1.62 m (91.11% recovery).

1.2. Hole M0096B

Deck operations and predeployment preparation were undertaken from 0000 to 0240 h on 6 September 2023. PROD5 was deployed at 0240 h to a water depth of 739.1 m, and coring operations progressed in Hole M0096B with wash boring to 0.99 m, just above the equivalent cored depth reached in Hole M0096A. At 0615 h, the hole was abandoned following mechanical issues (magazine wobble and manifold leak). PROD5 was recovered to deck at 0720 h on 6 September.

No cores were recovered from Hole M0096B, and the total cored length was 0.99 m by wash boring.

1.3. Hole M0096C

Deck operations and predeployment preparations of PROD5 were undertaken from 0720 to 1700 h on 6 September 2023. PROD5 was launched at 1700 h to a water depth of 739.9 m. Starting at 1835 h, coring operations were carried out in Hole M0096C. The hole was wash bored to 0.88 meters below seafloor (mbsf), and rotary coring continued until 2155 h, when the hole was abandoned after a drill rod was dropped inside the PROD5 frame. Recovery to deck was achieved at 2350 h on 6 September. Deck operations commenced, core barrels were extracted for curation, and the dropped core barrel was removed from the PROD5 frame. No damage was caused to the equipment.

One core was recovered from Hole M0096C, with 0.88 m of wash boring, a total of 1.74 m cored, and a recovered core length of 0.45 m (52.33% recovery).

1.4. Hole M0096D

On 7 September 2023, PROD5 was launched at 0150 h, and rotary coring and casing for Hole M0096D commenced between 0430 and 1505 h at a water depth of 736.8 m. The hole was abandoned at 7.30 mbsf at 1505 h due to misalignment of tools. PROD5 was recovered to deck at 1550 h. Core barrels were offloaded for curation, and deck operations were carried out between 1550 and 1630 h before leaving Site M0096 to transit to Site M0097 at 1630 h on 7 September.

Four cores were recovered from Hole M0096D from 7.40 m of rotary coring, and the total recovered core length was 2.24 m (30.27% recovery).

1.5. Hole M0096E

The *MMA Valour* transited back to Site M0096 on 18 September 2023, arriving at 0454 h. PROD5 was deployed at 1400 h but had mechanical issues (water ingress) and was retrieved back to deck. PROD5 was redeployed at 2013 h but had further mechanical problems with the port motor and was recovered on deck at 2035 h on 18 September. On 19 September, PROD5 was deployed at 1900 h to a water depth of 738.2 m and coring commenced at 2131 h. Hole M0096E was wash bored to 6.90 mbsf, close to the comparable deepest stratigraphic depth previously achieved at Site M0096. The hole was abandoned at 2310 h due to a manifold error, and after delays due to a fault with the winch level wind sensors, PROD5 was recovered to deck at 0119 h on 20 September.

No core was recovered from Hole M0096E.

1.6. Hole M0096F

Following checks of the manifold and compensation systems, at 0415 h on 20 September 2023, PROD5 was launched to a water depth of 738.2 m. Hole M0096F was wash bored to 6.70 mbsf

between 0605 and 1135 h. From 1135 to 1920 h, Hole M0096F was advanced by rotary coring and casing to 12.20 mbsf until a fault occurred with a drill head valve and the hole was abandoned. The 7.50 m of casing was removed, and PROD5 was recovered to deck at 2010 h for deck operations, core barrel extraction, and maintenance.

Five cores were recovered from Hole M0096F. A total of 5.52 m was advanced by wash boring, and 6.72 m of rotary coring was achieved. The total recovered core length was 4.76 m (86.23% recovery).

2. Lithostratigraphy

Site M0096 in the Kawaihae region consists of four holes (M0096A, M0096C, M0096D, and M0096F; Figure **F1**) taken at 740.8, 739.9, 736.8, and 738.2 mbsl, respectively. The first three holes consist primarily of mixed carbonate-volcaniclastic sediments, bioclastic materials (including corals and coralline algae), and large, subangular to subrounded volcanic clasts of variable crystallinity. In-place lava rock was recovered at the base of Hole M0096D (Sections 3R-2 and 4R-1). The fourth hole (M0096F) consists entirely of in-place lava rock with flow-induced texture, variable vesicularity, and low crystallinity, as well as lava clinker, which is common for subaerial emplacement conditions.

2.1. Hole M0096A

In Hole M0096A, mixed carbonate-volcaniclastic sediment was recovered from 0.00 to 1.49 mbsf and lava was recovered from 1.49 to 1.66 mbsf (Figure **F2**). The carbonate-volcaniclastic sediment is a conglomerate of poorly rounded sand- to cobble-sized clasts of phaneritic and aphanitic lava, corals, crustose coralline algae (CCA), *Halimeda* plates, and other carbonate components. Most coral fragments are *Porites* branches, one massive *Porites*, and one *Pocillopora* branch. All volcanic clasts are rounded to subrounded. The porphyritic lava clasts have visible crystals of clinopyroxene and olivine in a phaneritic matrix, are generally dense (<5% vesicularity), and contain polygonal networks of secondary infilled cracks. The aphanitic lava clasts contain fewer phenocrysts (<5%) and contain two types of vesicles (several millimeters to 1 cm elongated and rounded to subrounded 1–5 mm vesicles). In most porphyritic lava clasts, a fine-grained, brown matrix makes up approximately 40% of the rock volume. The base of the hole (Section 2R-2) consists of two clasts of different lithologies (Figure **F3**). The first is an upper aphanitic basalt clast with rounded 2–5 mm vesicles, small olivine and clinopyroxene phenocrysts concentrated near the outer margins, and carbonate-filled cracks and a few rounded vesicles. The lower clast is a porphyritic picrite with approximately 50 vol% of subeuhedral to euhedral crystals, primarily of

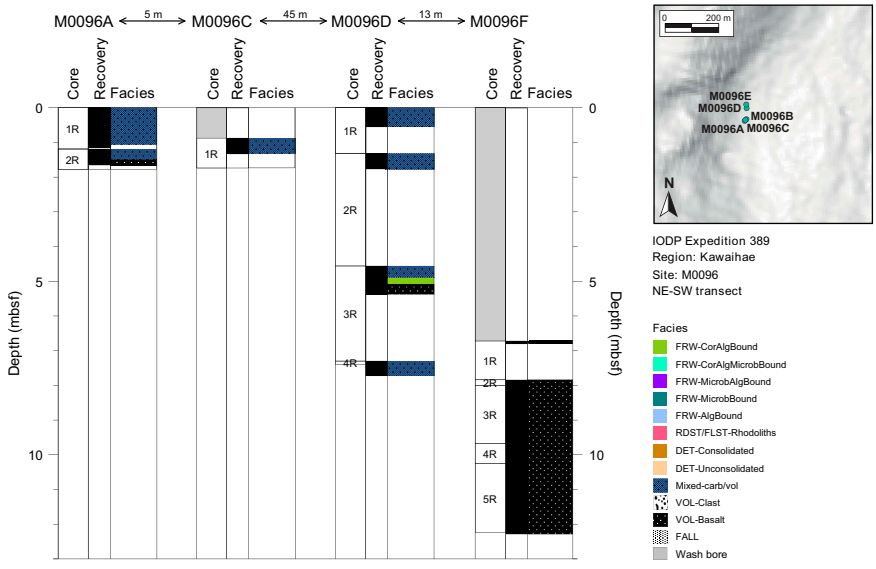

Figure F1. Lithostratigraphy, Site M0096.

olivine, with lesser amounts of clinopyroxene. The lower clast also has a notable Fe oxide and clay-rich rind that is <1 mm thick.

2.2. Hole M0096B

This hole was cored by wash bore only; no core was recovered (Table **T1**).

2.3. Hole M0096C

In Hole M0096C, nothing was recovered from 0 to 0.88 mbsf. Granule- to pebble-sized fragments of lava rock, *Halimeda* grainstone, CCA, and corals (*Porites* and one *Montipora*) were recovered from 0.88 to 1.33 mbsf (Figure **F4**). There are multiple lava clasts with highly variable lithologies in the core. All lava clasts are subrounded to subangular and vary from dense, low-vesicularity, low-phenocryst varieties with visually fresh-appearing groundmass to significantly altered and with significant Fe oxide replacement products in the groundmass. Clasts near the bottom of the section are more vesicular and more crystal rich than those in the upper part of the section. A

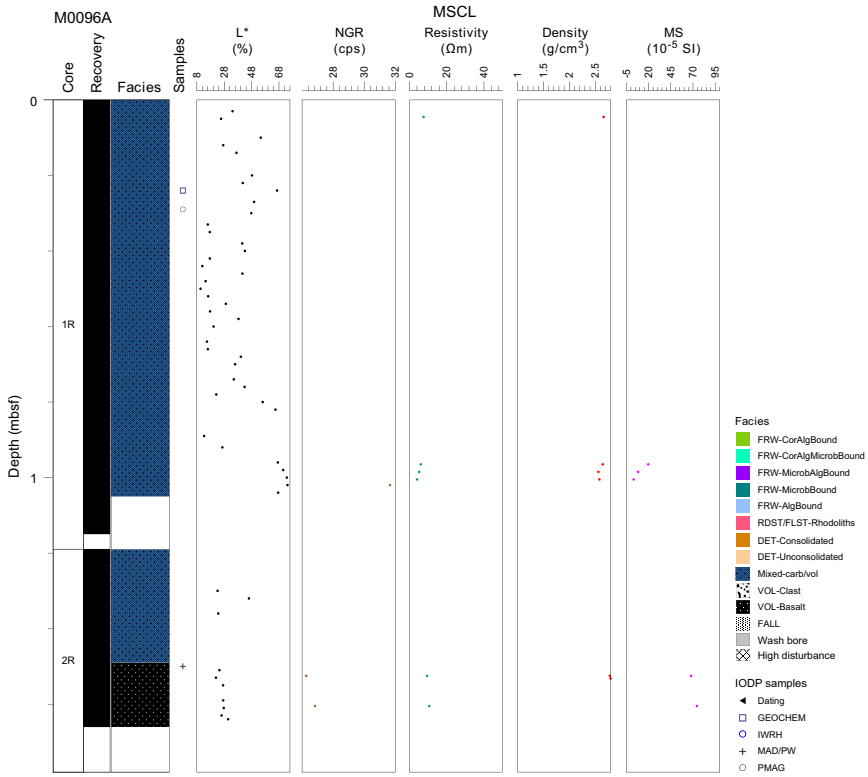

Figure F2. Lithostratigraphy and MSCL data, Hole M0096A. cps = counts per second, MS = magnetic susceptibility.

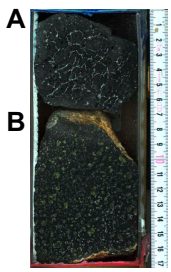

Figure F3. Lava lithologies, Hole M0096A (2R-2, 0–17 cm). A. Aphanitic lava clast with rounded 2–5 mm vesicles, small olivine, and clinopyroxene that are phenocrysts concentrated near the outer margins, as well as carbonate-filled cracks and a few rounded bubbles. B. Porphyritic picrite (approximately 50 vol% of subhedral to euhedral olivine crystals with lesser amounts of clinopyroxene) and a <1 mm thick Fe oxide– and clay-rich rind.

picrobasaltic lava clast at 1.19–1.23 mbsf (Figure **F5**) has variable features. The interior portion is a pristine looking lava rock with 10%–15% crystallinity and round vesicles. There is a sharp boundary to a highly altered (carbonate and Fe oxide replacement) exterior rind with similar crystallinity and vesicularity.

2.4. Hole M0096D

In Hole M0096D, mixed carbonate-volcaniclastic sediment, coralgal boundstone, and lava were retrieved from 0 to 7.72 mbsf (Figure **F6**). The lava clasts in this core are highly variable in size, shape, composition, texture, and freshness, ranging from fresh, low-vesicularity picrobasalt lava with a high phenocryst content to highly altered lavas with and without phenocrysts. Most lava clasts contain round to subrounded vesicles. The uppermost 0.22 m is a conglomerate of granule- to pebble-sized lava fragments, coral (*Porites*), CCA, and *Halimeda* grainstone clasts in a coarse sandy matrix. Below this depth (Section 1R-1), the core is disturbed with fragments of the above facies. From 0.22 to 4.91 mbsf, clasts of aphanitic and phaneritic lava, CCA, corals (*Porites* and *Pocillopora*), and gastropod shells occur. A short interval (4.91–5.08 mbsf) of coralgal boundstone containing *Porites* and coralline algal crusts lies above an interval (5.08–5.38 mbsf) of aphanitic lava with olivine crystals and cracks. Section 3R-2 consists primarily of a contiguous volcanic unit from 5.15 to 5.38 mbsf that is either in-place lava rock or a very large, visually unoxidized clast with millimeter to submillimeter rounded vesicles, olivine microphenocrysts, and an inclined,

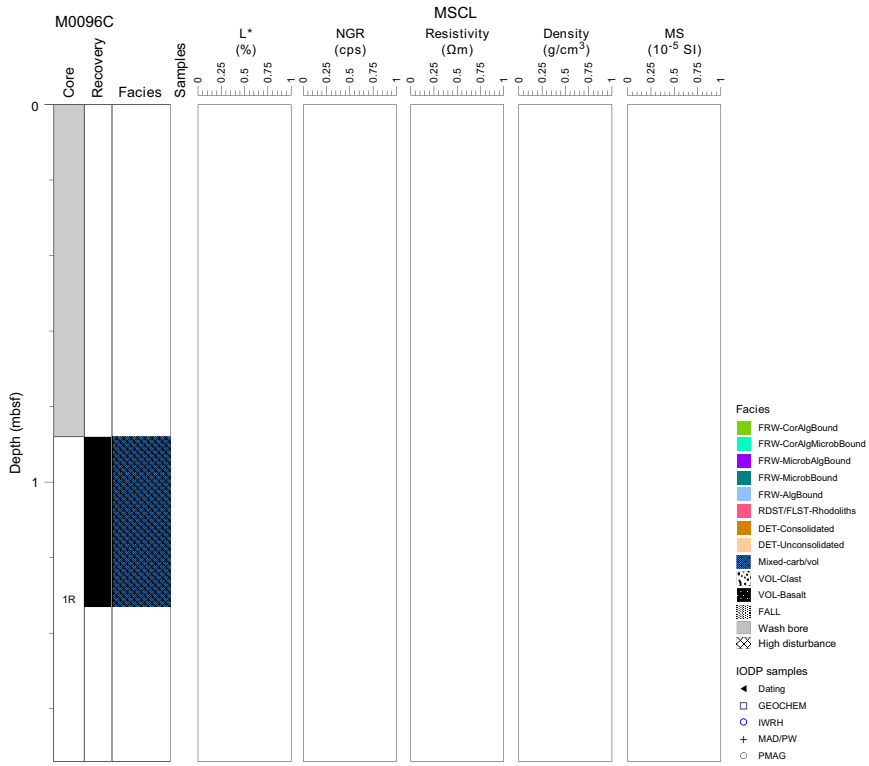

Figure F4. Lithostratigraphy and MSCL data, Hole M0096C. No physical properties data are available for this hole (see text for explanation). cps = counts per second, MS = magnetic susceptibility.

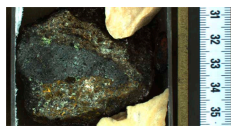

Figure F5. Lithologies, Hole M0096C. Picrobasalt lava clast consisting of a 10%–15% crystallinity interior with round vesicles (389-M0096C-1R-1, 31–35 cm). It has a visually fresh interior and a highly altered (calcium carbonate and Fe oxide replacement) rind.

calcite-infilled matrix crack zone. It is overlain by a thin layer (1–3 cm thick) consisting of highly vesicular, aphanitic, visibly altered rounded lava clasts with substantial infilling of vesicles, primarily by calcium carbonate precipitate and a variety of small detrital grains (Figure **F7**). The base of the core (7.30–7.72 mbsf) consists of mixed carbonate-volcaniclastic sediment with fragments of corals (*Porites*), CCA, and lava.

2.5. Hole M0096E

This hole was cored by wash bore only; no core was recovered (Table **T1**).

2.6. Hole M0096F

Hole M0096F is substantially different than the others at this site (Figure **F8**). There is no recovery from 0 to 6.72 mbsf. The interval between 6.72 and 8.09 mbsf consists of a thin clastic layer (Sections 1R-1 and 2R-1) of a mixed lava assemblage of variable vesicularity, phenocryst abundance, phenocryst content (olivine ± pyroxene), rounding, and alteration. This mixed, clastic zone grades into an in-place ʻaʻa lava rock sequence in Section 3R-1. This in-place lava with flow texture is aphanitic and highly vesicular. Most of it is visually fresh with open but unornamented vesicle linings. There is a notable zone containing calcium carbonate–infilled vesicles and Fe oxide staining between 8.31 and 8.41 mbsf in this section (Figure **F9A**) and another interval at roughly 8.70 mbsf. The lava terminates abruptly at 9.00 mbsf (Figure **F9B**) into a 6 cm thick, highly altered zone

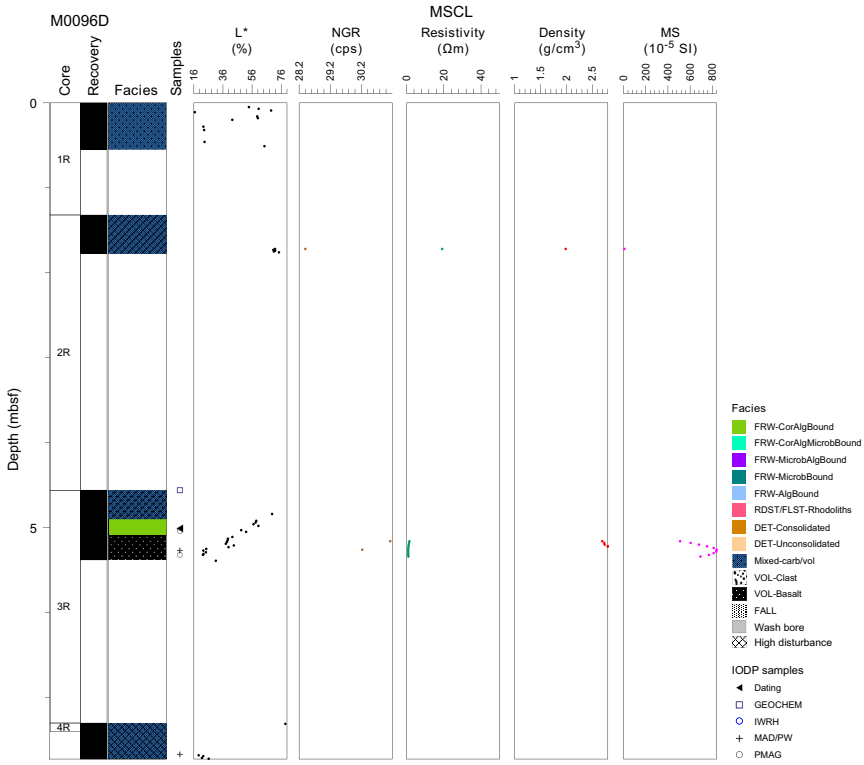

Figure F6. Lithostratigraphy and MSCL data, Hole M0096D. cps = counts per second, MS = magnetic susceptibility.

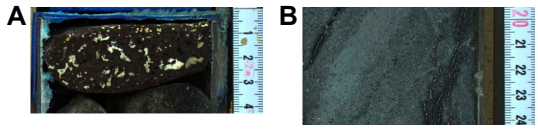

Figure F7. Lithologies, Hole M0096D. (A) Highly vesicular, aphanitic, visibly altered rounded lava clast with substantial infilling of vesicles, primarily by calcite, and a variety of small detrital grains (3R-2, 0–4 cm) overlying (B) dense, low-vesicularity, fresh lava (3R-2, 20–24 cm).

with extensive bioclastic and siliciclastic deposition in vugs and voids of the lava rock, which overlies a highly variable rounded to subrounded autobreccia of aphanitic, vesicular lava of variable alteration. This altered zone lacks any calcite precipitates and has notable variation in matrix color (orange to black), indicating alteration under oxidizing conditions. This ‘a‘a clinker texture continues into Section 3R-2, although the extent of alteration increases with depth. The clinker texture continues through the top of Section 4R-1, back into fresh, vesicular ‘a‘a lava rock at 9.95 mbsf in the same section (Figure **F9C**). The rest of Section 4R-1 grades between coherent, aphanitic, generally phenocryst free, vesicular ‘a‘a lava rock and partially agglutinated subrounded clinker of variable freshness and vesicle infilling. Although texturally similar throughout Sections 3R-1 through 5R-2 (i.e., the contiguous bottom sections), the abrupt change in the macroscopic appearance of the lava rock and alteration at 9.00 mbsf indicates a substantial change in emplacement and alteration conditions, representing either a boundary between two discrete lava rock units with flow textures or a boundary within lobes of a compound lava flow rock unit that experienced sufficient time between lobe emplacement for a discrete alteration boundary to develop.

X-ray fluorescence analysis of three lava samples from Site M0096 is broadly consistent with lava composition, variable degrees of alteration, and differences in primary phenocryst accumulation between specimens of the same primary magma deposit (see **Geochemistry**). There are insufficient data to constrain potential petrologic differences in source or fractionation history. X-ray diffraction (XRD) analysis of the same three samples indicates variable primary and secondary mineralogy. One sample (389-M0096F-04R-1, 16–17 cm; Figure **F10**) is moderately altered lava containing abundant calcium carbonate precipitates as vesicle infilling, whereas the lava contains abundant common primary igneous basaltic minerals. The lava also contains volumetrically minor quantities of a high-temperature silica polymorph, clay, and zeolite.

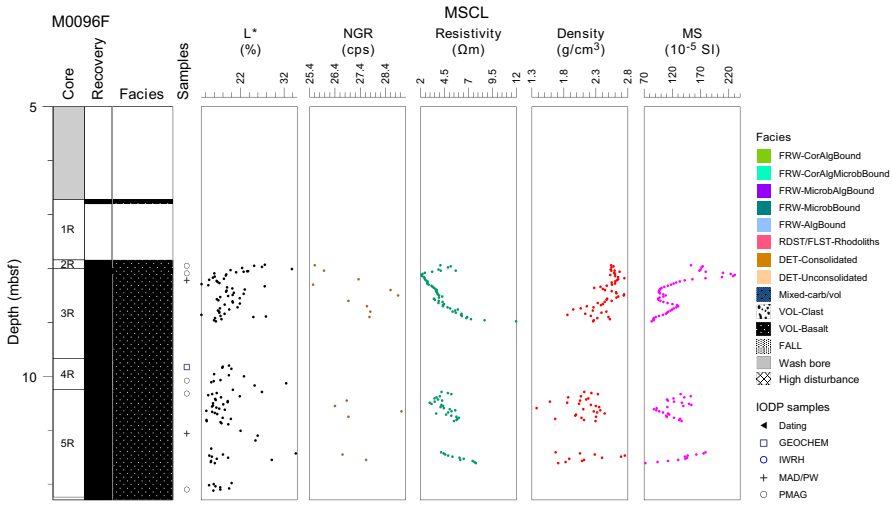

Figure F8. Lithostratigraphy and MSCL data, Hole M0096F. cps = counts per second, MS = magnetic susceptibility.

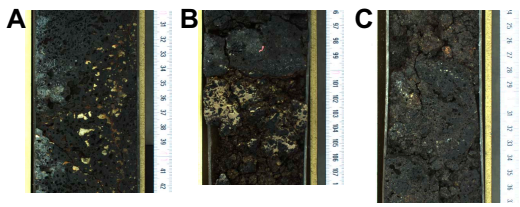

Figure F9. Lithologies, Hole M0096F. A. In-place lava potentially representing a lava flow with a zone of Fe oxide staining and calcium carbonate-infilled vesicles (3R-1, 30–42 cm). B. Sharp contact between a visually fresh lava with lava flow textures overlying a highly altered lava with angular to rounded clasts in a sediment-supported matrix underlain by an autobreccia of aphanitic, vesicular lava of variable alteration and matrix color (ranging from orange to black) (3R-1, 96–108 cm). C. Slightly altered, vesicular, basaltic ‘a‘a lava rock with irregular vesicle sizes and shapes arranged radially within the clast (4R-1, 24–37 cm).

Figure F10. Altered lava rock fragment analyzed using XRD (389-M0096F-4R-1, 15–18 cm) (see Geochemistry). Red box = geochemical sampling location.

3. Physical properties

Physical properties data for Site M0096 are shown in Table **T2**.

3.1. Hole M0096A

A total of 1.52 m of core from Hole M0096A was scanned with the multisensor core logger (MSCL), and the core exhibited major drilling-induced disturbance, resulting in only 6% of the acquired data passing QA/QC (see Table **T10** in the Expedition 398 methods chapter [Webster et al., 2025]). One discrete sample was taken for *P*-wave velocity and moisture and density (MAD) measurements. Digital linescans, color reflectance, and hyperspectral imaging were acquired on all cores.

3.1.1. Density and porosity

Density and porosity data are presented in Figures **F2** and **F11** and Table **T2**. MSCL bulk density values range 2.56–2.97 g/cm^3. Drilling-induced disturbance and short core lengths compromised data quality (see **Physical properties** in the Expedition 389 methods chapter [Webster et al., 2025]) and limited sampling. However, one discrete sample was analyzed for MAD, giving a bulk density value of 2.88 g/cm^3. The porosity value for this sample is 5.3%, and the grain density value is 2.986 g/cm^3.

3.1.2. *P*-wave velocity

P-wave velocity measurements on the MSCL yielded no data. One sample was measured using the discrete *P*-wave logger. The dry measurement value is 4758 m/s (Figure **F12**). *P*-wave velocity recorded for the same sample after resaturation is 6366 m/s. Because only one *P*-wave data point is available for Hole M0096A, there are no apparent downhole trends.

3.1.3. Thermal conductivity

Because of the presence of drilling-induced disturbances, large voids, and uneven surfaces, thermal conductivity measurements were not performed on Hole M0096A cores.

3.1.4. Magnetic susceptibility

MSCL magnetic susceptibility data range 3.09×10^{-5} to 74.43×10^{-5} SI (Figure **F2**). Even though there are only five measurements available, the values reflect the lithology, with lower values in the upper mixed carbonate-volcaniclastic sediment and markedly higher values in the lava at the base.

3.1.5. Electrical resistivity

MSCL noncontact resistivity measurements range 4.02–10.63 Ωm (Figure **F2**). Similar to the other data sets for this hole, despite the limited data available, the change in lithology is reflected by higher values in the lava at the base of the hole.

3.1.6. Natural gamma radiation

MSCL natural gamma radiation (NGR) measurements range 26–32 counts/s and because of limited data points show no apparent downhole trends (Figure **F2**).

3.1.7. Digital linescans, color reflectance, and hyperspectral imaging

Cores were digitally scanned, measured for color reflectance (where appropriate), and imaged with the hyperspectral scanner (see HYPERSPECTRAL in **Supplementary material**). Color reflectance L* values vary between 10.71% and 74.19%, a* varies between –1.26 and 4.50, b* varies

Table T2. Physical properties summary, Expedition 389. MSCL = whole-round core, MAD = discrete sample. SD = standard deviation. — = not measured. (Continued on next two pages.) **Download table in CSV format.**

Hole	Value	MSCL				MAD		
		Magnetic susceptibility (10^{-5} SI)	Electrical resistivity (Ωm)	NGR (cps)	Bulk density (g/cm³)	Bulk density (g/cm³)	Porosity (%)	Grain density (g/cm³)
389-								
M0096A	Min	3.09	4.02	26	2.56	2.88	5.3	2.986
	Max	74.43	10.63	32	2.97	2.88	5.3	2.986
	Mean ± SD	34.64 ± 30.37	7.16 ± 2.32	28 ± 2	2.70 ± 0.14	—	—	—
M0096D	Min	7.34	0.90	28	1.99	2.65	8.8	2.913
	Max	839.44	19.13	31	1.99	2.75	19.9	3.058
	Mean ± SD	665.00 ± 230.14	2.71 ± 5.19	30 ± 1	—	2.70 ± 0.07	14.4 ± 7.9	2.985 ± 0.103
M0096F	Min	72.20	2.11	26	1.37	2.56	17.7	2.956
	Max	230.53	11.97	29	2.75	2.70	20.6	3.067
	Mean ± SD	127.00 ± 34.10	4.60 ± 1.60	27 ± 1	2.31 ± 0.29	2.63 ± 0.11	19.2 ± 2.1	3.011 ± 0.080
M0097A	Min	−1.48	1.01	27	0.14	1.90	7.7	2.100
	Max	97.83	173.72	36	2.68	2.67	35.8	2.886
	Mean ± SD	1.45 ± 10.03	12.61 ± 13.08	31 ± 2	2.24 ± 0.26	2.38 ± 0.17	21.5 ± 7.0	2.757 ± 0.165
M0097B	Min	−3.30	1.96	24	0.19	2.21	12.3	2.545
	Max	2.36	64.48	35	2.59	2.55	29.2	2.836
	Mean ± SD	−1.13 ± 0.80	7.58 ± 4.26	30 ± 2	2.25 ± 0.26	2.40 ± 0.09	20.5 ± 4.9	2.755 ± 0.063
M0097C	Min	−4.17	1.88	26	0.91	2.24	9.2	2.748
	Max	86.47	247.30	35	2.6	2.68	30.4	2.849
	Mean ± SD	0.08 ± 6.80	9.18 ± 14.38	30 ± 2	2.27 ± 0.22	2.48 ± 0.09	17.6 ± 4.8	2.787 ± 0.036
M0097D	Min	−1.28	1.12	26	0.53	2.35	14.8	2.733
	Max	132.62	260.57	35	2.56	2.51	26.4	2.850
	Mean ± SD	1.51 ± 12.05	9.36 ± 15.01	30 ± 2	2.14 ± 0.31	2.44 ± 0.05	19.4 ± 3.8	2.778 ± 0.042
M0098A	Min	−0.61	1.46	31	1.28	2.31	26.7	2.781
	Max	8.88	51.80	37	2.56	2.31	26.7	2.781
	Mean ± SD	2.86 ± 2.84	12.99 ± 13.81	35 ± 2	2.13 ± 0.28	—	—	—
M0099A	Min	−1.02	2.89	25	1.78	2.28	17.4	2.772
	Max	12.05	49.79	28	2.52	2.47	28.3	2.776
	Mean ± SD	0.35 ± 2.66	8.35 ± 7.32	26 ± 1	2.21 ± 0.16	2.35 ± 0.10	22.9 ± 5.8	2.774 ± 0.002
M0099B	Min	−1.55	2.22	25	1.84	2.34	21.5	2.738
	Max	−0.48	22.66	28	2.46	2.37	27.1	2.850
	Mean ± SD	−1.04 ± 0.27	6.28 ± 3.03	26 ± 1	2.20 ± 0.14	2.36 ± 0.01	24.4 ± 2.8	2.786 ± 0.058
M0099C	Min	−3.36	0.79	23	0.54	2.27	14.6	2.726
	Max	70.58	52.66	30	2.52	2.48	30.0	2.804
	Mean ± SD	0.33 ± 5.59	4.83 ± 3.68	26 ± 2	2.12 ± 0.25	2.38 ± 0.07	22.0 ± 4.8	2.760 ± 0.023
M0099E	Min	−0.94	1.07	24	1.37	1.93	10.3	2.741
	Max	35.87	389.45	31	2.63	2.57	53.1	2.953
	Mean ± SD	0.21 ± 4.39	12.93 ± 26.98	27 ± 1	2.15 ± 0.26	2.37 ± 0.22	23.8 ± 14.8	2.807 ± 0.076
M0099F	Min	−0.54	1.58	24	1.57	2.43	9.2	2.747
	Max	0.74	49.02	29	2.56	2.59	20.4	2.789
	Mean ± SD	−0.01 ± 0.23	5.68 ± 6.02	26 ± 1	2.11 ± 0.23	2.51 ± 0.11	14.8 ± 4.0	2.768 ± 0.015
M0099G	Min	−0.80	0.93	25	1.23	2.07	8.4	2.750
	Max	798.19	120.62	34	2.89	2.73	47.8	3.024
	Mean ± SD	129.04 ± 199.25	5.99 ± 8.90	29 ± 2	2.26 ± 0.33	2.38 ± 0.23	26.4 ± 11.9	2.872 ± 0.088
M0100A	Min	20.39	1.42	27	1.02	2.29	14.1	2.646
	Max	540.81	124.53	35	2.80	2.51	24.8	2.862
	Mean ± SD	165.14 ± 79.20	4.69 ± 8.91	31 ± 2	2.36 ± 0.32	2.38 ± 0.09	20.3 ± 4.0	2.730 ± 0.081
M0101A	Min	5.31	1.06	30	1.15	2.14	21.1	2.787
	Max	259.00	26.16	46	2.57	2.49	36.9	2.884
	Mean ± SD	49.54 ± 59.98	4.94 ± 3.25	36 ± 5	2.01 ± 0.30	2.33 ± 0.18	27.5 ± 8.3	2.820 ± 0.055
M0101B	Min	4.24	0.43	25	1.56	1.55	5.7	2.517
	Max	1548.13	22.45	47	2.97	2.82	70.5	3.068
	Mean ± SD	443.40 ± 295.06	1.82 ± 1.32	30 ± 3	2.51 ± 0.31	2.41 ± 0.49	28.2 ± 22.5	2.923 ± 0.162
M0102A	Min	2.55	0.52	25	0.69	1.82	27.4	2.669
	Max	1290.01	19.12	38	2.60	2.35	53.7	2.864
	Mean ± SD	86.62 ± 122.34	1.91 ± 1.82	32 ± 2	2.02 ± 0.19	2.00 ± 0.22	44.7 ± 10.6	2.776 ± 0.084
M0102C	Min	−1.68	0.46	25	1.08	1.75	10.6	2.294
	Max	267.75	39.82	45	2.61	2.64	60.7	2.907
	Mean ± SD	74.75 ± 53.69	2.99 ± 2.20	31 ± 2	2.11 ± 0.24	2.30 ± 0.22	28.0 ± 11.6	2.802 ± 0.107
M0103A	Min	−0.67	0.33	26	1.48	2.17	8.1	2.717
	Max	330.12	47.04	38	2.59	2.85	34.3	3.007
	Mean ± SD	26.89 ± 65.46	2.54 ± 4.28	32 ± 3	2.04 ± 0.21	2.35 ± 0.23	25.1 ± 8.4	2.786 ± 0.099
M0104A	Min	−0.74	0.98	25	0.11	2.09	13.4	2.723
	Max	126.30	53.97	34	2.69	2.52	40.4	2.850
	Mean ± SD	8.68 ± 18.24	7.65 ± 4.73	30 ± 2	2.24 ± 0.29	2.39 ± 0.10	21.9 ± 5.9	2.769 ± 0.027

Table T2 (continued). (Continued on next page.)

Hole	Value	MSCL				MAD		
		Magnetic susceptibility (10^{-5} SI)	Electrical resistivity (Ωm)	NGR (cps)	Bulk density (g/cm^3)	Bulk density (g/cm^3)	Porosity (%)	Grain density (g/cm^3)
M0105A	Min	–0.41	1.05	26	1.71	2.12	14.2	2.770
	Max	487.32	20.12	32	3.03	2.84	40.4	3.192
	Mean ± SD	217.38 ± 103.11	3.73 ± 2.8	29 ± 1	2.54 ± 0.28	2.58 ± 0.33	23.9 ± 10.4	3.050 ± 0.183
M0106A	Min	0.67	6.45	26	1.71	2.29	25.7	2.732
	Max	4.99	20.80	26	2.22	2.29	25.7	2.732
	Mean ± SD	1.87 ± 1.49	11.22 ± 4.37	—	2.09 ± 0.15	—	—	—
M0106B	Min	–0.73	0.84	26	1.46	—	—	—
	Max	6.59	7.85	28	2.12	—	—	—
	Mean ± SD	3.60 ± 2.26	3.32 ± 1.89	27 ± 1	1.78 ± 0.15	—	—	—
M0107A	Min	6.25	1.73	24	0.99	2.57	10.8	2.804
	Max	313.91	15.98	31	2.89	2.74	18.5	3.040
	Mean ± SD	159.08 ± 78.16	4.11 ± 1.95	27 ± 1	2.63 ± 0.18	2.65 ± 0.06	14.4 ± 2.5	2.924 ± 0.082
M0108A	Min	—	—	—	—	—	—	—
	Max	—	—	—	—	—	—	—
	Mean ± SD	—	—	—	—	—	—	—
M0108B	Min	–0.67	0.62	29	1.39	—	—	—
	Max	0.60	23.74	37	2.33	—	—	—
	Mean ± SD	–0.23 ± 0.23	4.17 ± 4.25	33 ± 2	1.99 ± 0.15	—	—	—
M0109A	Min	0.06	1.47	31	1.44	—	—	—
	Max	4.17	16.69	39	2.15	—	—	—
	Mean ± SD	1.11 ± 1.12	4.55 ± 4.53	34 ± 4	1.95 ± 0.15	—	—	—
M0110A	Min	–0.81	0.89	24	1.45	2.10	4.2	2.660
	Max	460.73	354.16	35	2.90	2.82	40.3	2.901
	Mean ± SD	100.91 ± 122.69	10.46 ± 20.7	31 ± 3	2.30 ± 0.32	2.47 ± 0.24	18.3 ± 12.6	2.797 ± 0.080
M0110B	Min	–0.61	0.24	25	1.79	2.10	5.9	2.766
	Max	3525.64	42.64	38	2.90	2.87	38.5	3.129
	Mean ± SD	1270.42 ± 840.46	1.79 ± 4.05	33 ± 3	2.46 ± 0.23	2.60 ± 0.25	17.9 ± 9.8	2.941 ± 0.133

Hole	Value	Discrete *P*-wave velocity			Section-half				
		Initial (m/s)	Dry (m/s)	Resaturated (m/s)	Thermal conductivity (W/[m·K])	L* (%)	a*	b*	a*/b*
389-									
M0096A	Min	5030	4758	6366	—	10.71	–1.26	–0.86	–0.38
	Max	5030	4758	6366	—	74.19	4.50	21.57	1.54
	Mean ± SD	—	—	—	—	35.37 ± 14.84	0.82 ± 1.52	7.22 ± 6.05	0.05 ± 0.22
M0096D	Min	5058	2828	4123	1.793	16.67	–1.31	0.60	–2.08
	Max	5144	5228	7202	1.793	78.87	3.82	20.16	0.25
	Mean ± SD	5101 ± 61	4028 ± 1697	5662 ± 2178	—	45.28 ± 17.09	0.63 ± 1.28	8.63 ± 6.25	–0.22 ± 0.42
M0096F	Min	4370	3622	4253	1.533	13.05	–1.00	–0.65	–0.59
	Max	4933	3908	4742	1.533	34.68	2.76	12.25	0.31
	Mean ± SD	4651 ± 399	3765 ± 202	4497 ± 345	—	19.03 ± 3.09	–0.20 ± 0.37	3.84 ± 1.37	–0.10 ± 0.11
M0097A	Min	3230	1754	3122	1.290	15.68	–0.48	3.05	–0.12
	Max	5946	5275	5804	1.314	87.04	5.78	23.47	0.36
	Mean ± SD	4413 ± 790	3727 ± 822	4302 ± 680	1.303 ± 0.012	71.74 ± 4.71	1.30 ± 0.61	16.40 ± 1.49	0.07 ± 0.03
M0097B	Min	4142	3389	3723	1.286	47.54	–1.33	5.66	–0.21
	Max	5217	5034	5350	1.286	85.27	3.14	20.48	0.16
	Mean ± SD	4712 ± 293	4305 ± 529	4556 ± 486	—	70.23 ± 4.54	0.58 ± 0.51	15.48 ± 1.79	0.03 ± 0.03
M0097C	Min	3838	2779	2965	1.248	39.36	–0.41	6.69	–0.04
	Max	6202	6164	6629	1.657	86.88	7.82	24.8	0.41
	Mean ± SD	4981 ± 622	4178 ± 955	4442 ± 771	1.427 ± 0.209	73.52 ± 3.65	1.77 ± 0.61	17.32 ± 1.79	0.09 ± 0.02
M0097D	Min	3947	3527	3245	—	26.55	–0.62	1.30	–0.33
	Max	5674	4847	5009	—	89.84	6.14	21.99	0.45
	Mean ± SD	4815 ± 499	4243 ± 378	4627 ± 466	—	74.57 ± 4.29	1.72 ± 0.55	16.95 ± 1.91	0.09 ± 0.02
M0098A	Min	—	—	3789	—	30.32	–0.63	8.78	–0.06
	Max	—	—	3789	—	78.33	7.61	26.23	0.29
	Mean ± SD	—	—	—	—	68.40 ± 4.93	1.67 ± 1.27	16.31 ± 3.14	0.08 ± 0.05
M0099A	Min	5231	4606	3289	—	62.71	–0.50	10.22	–0.03
	Max	5231	4606	4753	—	86.34	2.82	19.91	0.15
	Mean ± SD	—	—	4046 ± 733	—	73.90 ± 3.65	0.76 ± 0.82	16.43 ± 1.67	0.04 ± 0.02
M0099B	Min	3849	3812	3792	—	62.88	–1.02	12.20	–0.08
	Max	4735	3837	3993	—	82.09	2.43	20.06	0.14
	Mean ± SD	4292 ± 626	3827 ± 13	3910 ± 105	—	73.72 ± 3.90	0.70 ± 0.41	16.73 ± 1.13	0.04 ± 0.02

Table T2 (continued).

Hole	Value	Discrete *P*-wave velocity			Section-half				
		Initial (m/s)	Dry (m/s)	Resaturated (m/s)	Thermal conductivity (W/[m·K])	L* (%)	a*	b*	a*/b*
M0099C	Min	3673	3078	3343	1.137	33.84	−1.23	−1.08	−0.25
	Max	5068	4864	5258	1.309	87.65	4.20	22.50	0.20
	Mean ± SD	4489 ± 512	4044 ± 496	4188 ± 503	1.220 ± 0.086	74.47 ± 4.50	0.72 ± 0.44	15.47 ± 1.61	0.04 ± 0.02
M0099E	Min	3597	2990	3500	1.280	30.13	−0.72	8.02	−0.06
	Max	6056	4620	5425	1.280	88.81	3.34	20.6	0.18
	Mean ± SD	5013 ± 696	4116 ± 528	4631 ± 692	—	73.53 ± 4.77	0.73 ± 0.49	15.56 ± 1.57	0.04 ± 0.02
M0099F	Min	4570	4052	4441	1.012	43.69	−0.32	0.04	−1.50
	Max	5133	5108	5029	1.250	97.29	2.95	19.19	0.18
	Mean ± SD	4852 ± 398	4580 ± 747	4735 ± 416	1.131 ± 0.168	76.05 ± 5.36	0.89 ± 0.46	15.34 ± 1.45	0.04 ± 0.03
M0099G	Min	2400	1715	3196	0.989	4.85	−2.13	−0.91	−4.25
	Max	7297	5039	6040	1.880	84.94	15.31	19.49	1.87
	Mean ± SD	4697 ± 1399	3904 ± 1017	4594 ± 934	1.469 ± 0.397	45.68 ± 27.76	0.35 ± 0.86	8.97 ± 5.47	−0.05 ± 0.17
M0100A	Min	3475	2078	3051	1.505	10.12	−1.26	−0.81	−1.15
	Max	6204	4772	5136	1.505	97.26	4.17	18.09	3.88
	Mean ± SD	4817 ± 1081	3657 ± 1082	4170 ± 881	—	22.21 ± 8.45	0.36 ± 0.64	4.07 ± 2.54	0.06 ± 0.18
M0101A	Min	3797	1888	3842	—	14.61	−1.08	1.47	−0.15
	Max	3930	3361	4926	—	79.15	6.73	27.26	0.33
	Mean ± SD	3864 ± 94	2859 ± 841	4384 ± 766	—	48.49 ± 8.68	2.52 ± 1.30	15.12 ± 4.04	0.14 ± 0.07
M0101B	Min	4941	4316	4371	1.116	2.52	−1.28	−1.02	−5.50
	Max	6755	5494	7219	1.804	80.29	10.35	28.61	1.50
	Mean ± SD	5760 ± 598	4929 ± 411	5461 ± 840	1.578 ± 0.271	27.76 ± 14.85	0.79 ± 1.86	6.92 ± 6.26	−0.04 ± 0.35
M0102A	Min	4167	4078	4149	—	31.08	−1.31	2.17	−0.43
	Max	4167	4078	4149	—	74.35	5.33	20.07	0.31
	Mean ± SD	—	—	—	—	50.08 ± 7.31	−0.28 ± 0.50	8.06 ± 2.47	−0.06 ± 0.05
M0102C	Min	3363	3183	3066	1.388	18.72	−1.57	1.75	−0.30
	Max	5846	5229	5253	1.450	83.57	7.17	28.11	0.87
	Mean ± SD	4475 ± 569	3798 ± 459	4074 ± 543	1.419 ± 0.044	57.86 ± 12.63	−0.09 ± 0.37	10.52 ± 2.83	−0.01 ± 0.03
M0103A	Min	3680	3203	3678	—	16.62	−1.61	−0.53	−0.58
	Max	5130	4399	4682	—	85.60	5.99	28.69	0.34
	Mean ± SD	4252 ± 447	3822 ± 351	4104 ± 405	—	62.98 ± 8.97	0.49 ± 0.96	12.29 ± 2.93	0.01 ± 0.08
M0104A	Min	3014	3148	3384	1.126	30.51	−1.34	−1.13	−0.27
	Max	5768	5323	6076	1.529	87.52	9.19	32.58	0.42
	Mean ± SD	4553 ± 667	4150 ± 518	4777 ± 639	1.316 ± 0.167	67.53 ± 6.76	1.12 ± 1.40	15.19 ± 4.16	0.05 ± 0.08
M0105A	Min	3755	3257	3898	1.957	0.09	−1.94	−0.83	−1.78
	Max	6657	4626	5159	2.187	80.42	6.91	19.69	7.94
	Mean ± SD	5268 ± 1179	3856 ± 487	4480 ± 514	2.048 ± 0.122	26.55 ± 12.03	−0.11 ± 0.74	5.46 ± 3.03	−0.08 ± 0.22
M0106A	Min	4615	3892	4448	—	35.93	−1.02	4.48	−0.23
	Max	4615	3892	4448	—	64.79	1.77	14.10	0.14
	Mean ± SD	—	—	—	—	50.73 ± 5.24	0.37 ± 0.66	10.02 ± 2.07	0.02 ± 0.06
M0106B	Min	—	—	—	—	49.79	0.09	11.47	0.01
	Max	—	—	—	—	83.32	4.65	24.14	0.20
	Mean ± SD	—	—	—	—	71.68 ± 8.46	1.35 ± 0.80	15.36 ± 2.02	0.08 ± 0.04
M0107A	Min	6004	5014	5682	1.980	15.09	−0.86	1.73	−0.22
	Max	7426	6067	6078	2.126	72.29	5.08	23.82	0.28
	Mean ± SD	6800 ± 464	5623 ± 352	5838 ± 134	2.030 ± 0.083	42.04 ± 19.61	1.71 ± 1.81	11.85 ± 7.26	0.06 ± 0.13
M0108A	Min	—	—	—	—	67.92	0.39	11.51	0.03
	Max	—	—	—	—	78.66	1.97	18.60	0.11
	Mean ± SD	—	—	—	—	73.36 ± 2.78	1.28 ± 0.38	16.68 ± 0.98	0.07 ± 0.02
M0108B	Min	—	—	—	—	43.97	−1.02	6.49	−0.13
	Max	—	—	—	—	82.37	3.87	19.92	0.28
	Mean ± SD	—	—	—	—	69.84 ± 6.29	0.81 ± 0.70	14.01 ± 2.33	0.05 ± 0.03
M0109A	Min	—	—	—	—	56.39	0.53	9.46	0.04
	Max	—	—	—	—	77.61	2.58	22.24	0.15
	Mean ± SD	—	—	—	—	71.60 ± 2.92	1.56 ± 0.48	16.06 ± 2.01	0.09 ± 0.02
M0110A	Min	3669	3126	3316	1.148	9.43	−2.70	−2.06	−1.02
	Max	5845	5552	6789	1.676	83.72	4.81	22.23	3.60
	Mean ± SD	4871 ± 803	4389 ± 891	4881 ± 1287	1.385 ± 0.207	43.66 ± 25.69	0.77 ± 1.09	9.34 ± 5.57	0.06 ± 0.17
M0110B	Min	5144	2113	2942	1.683	8.99	−1.64	−1.28	−1.76
	Max	6861	5601	6090	1.706	82.13	3.67	24.38	1.00
	Mean ± SD	5966 ± 536	4696 ± 1114	5024 ± 959	1.695 ± 0.016	34.88 ± 22.70	0.01 ± 0.83	6.26 ± 5.11	−0.13 ± 0.25

between −0.86 and 21.57, and a*/b* varies between −0.38 and 1.54, with high variability in the mixed carbonate-siliciclastic sediment and consistently low values in the lava unit. (Figure **F2**).

3.2. Hole M0096B

This hole was cored by wash bore only; no core was recovered (Table **T1**).

3.3. Hole M0096C

Hole M0096C was not scanned with the MSCL, nor were any discrete samples taken. Only digital linescans of the working and archive halves were taken.

3.4. Hole M0096D

A total of 2.24 m of core from Hole M0096D was scanned with the MSCL, and the core exhibited major drilling-induced disturbance, resulting in 12% of the acquired data passing QA/QC (see Table **T10** in the Expedition 398 methods chapter [Webster et al., 2025]). Two discrete samples were taken for *P*-wave velocity and MAD measurements. Digital linescans, color reflectance, and hyperspectral imaging were acquired on all cores.

3.4.1. Density and porosity

Density and porosity data are presented in Figures **F6** and **F13** and Table **T2**. A single MSCL bulk density measurement of 1.99 g/cm^3 was recorded. Drilling-induced disturbances and short core lengths compromised the quality of the remaining density data (see **Physical properties** in the Expedition 389 methods chapter [Webster et al., 2025]) and limited sampling. However, two discrete samples were analyzed for MAD, giving bulk density values in the range of 2.65–2.75 g/cm^3. Porosity values for the same samples range 8.8%–19.9%, and grain density values fluctuate between 2.913 and 3.058 g/cm^3. There are no apparent downhole trends in the density and porosity data sets and no clear relationship between the two bulk density measurements (MSCL and discrete).

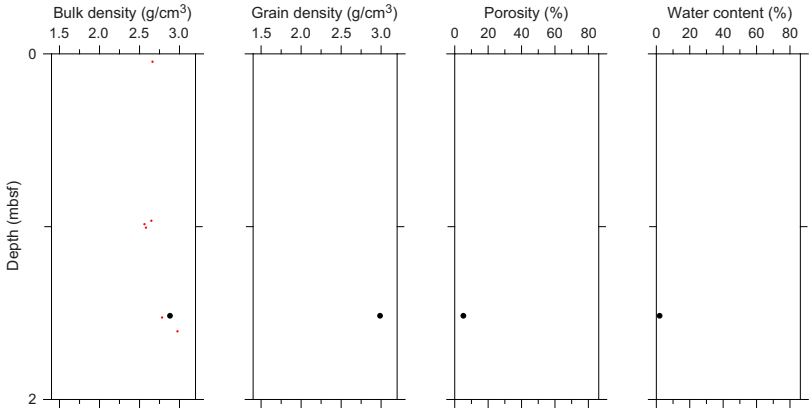

Figure F11. Physical properties, Hole M0096A. Black = discrete samples, red = MSCL.

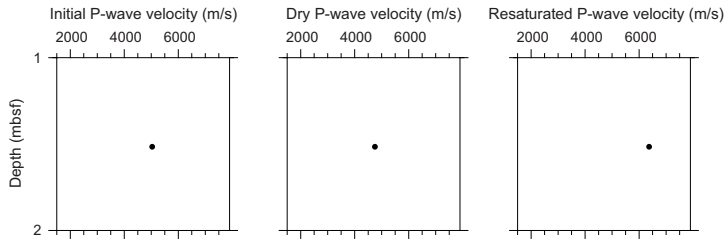

Figure F12. Initial, dry, and resaturated *P*-wave velocities measured on discrete samples, Hole M0096A.

3.4.2. *P*-wave velocity

MSCL *P*-wave velocity measurements yielded no data. Two samples were measured using the discrete *P*-wave logger. Dry measurement values are 2828 and 5228 m/s (Figure **F14**). *P*-wave velocities of 4123 and 7202 m/s were recorded for the resaturated samples. Because of the limited *P*-wave data points, it is not possible to detect downhole trends.

3.4.3. Thermal conductivity

Thermal conductivity was collected on one core (see Table **T11** in the Expedition 398 methods chapter [Webster et al., 2025]) and has a value of 1.793 W/(m·K).

3.4.4. Magnetic susceptibility

MSCL magnetic susceptibility data range 7.34×10^{-5} to 839.44×10^{-5} SI with mean values close to 665.00×10^{-5} SI (Figure **F15**).

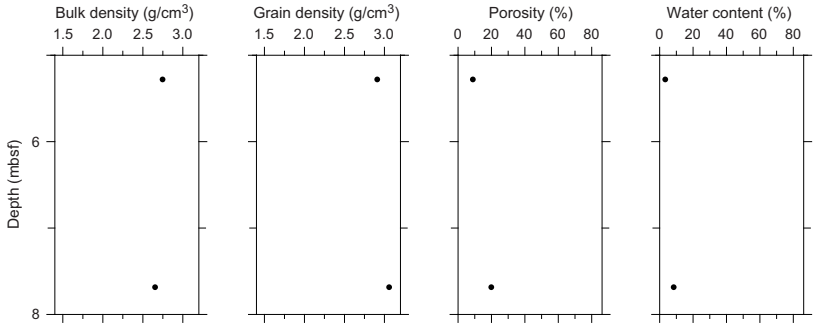

Figure F13. Physical properties, Hole M0096D. Black = discrete samples, red = MSCL.

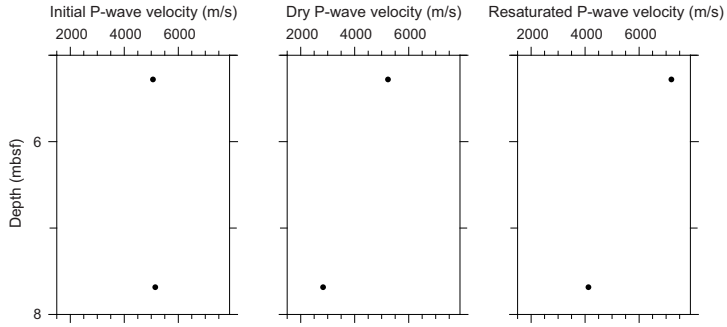

Figure F14. Initial, dry, and resaturated *P*-wave velocities measured on discrete samples, Hole M0096D.

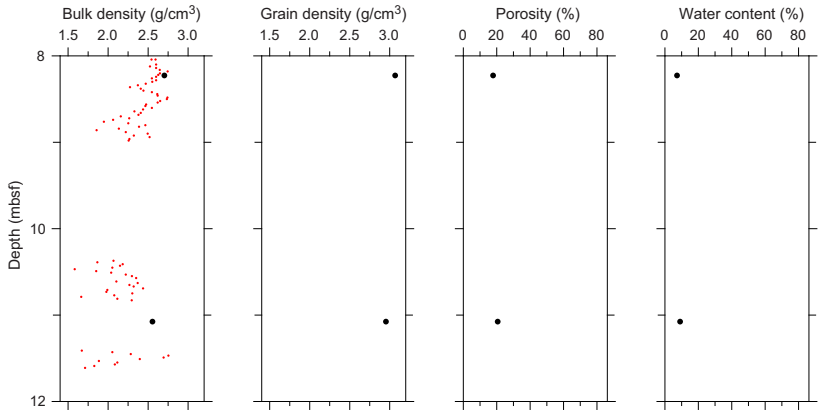

Figure F15. Physical properties, Hole M0096F. Black = discrete samples, red = MSCL.

3.4.5. Electrical resistivity

MSCL noncontact resistivity measurements yielded data ranging 0.90–19.13 Ωm (Figure **F6**). Similar to the other data sets for this hole, there are no apparent downhole trends.

3.4.6. Natural gamma radiation

MSCL NGR measurements display values ranging 28–31 counts/s and show no apparent downhole trends (Figure **F6**).

3.4.7. Digital linescans, color reflectance, and hyperspectral imaging

All cores were digitally scanned, and, where appropriate, measured for color reflectance and imaged with the hyperspectral scanner (see HYPERSPECTRAL in **Supplementary material**). Color reflectance L* values vary between 16.67% and 78.87%, a* varies between –1.31 and 3.82, b* varies between 0.60 and 20.16, and a*/b* varies between –2.08 and 0.25 (Figure **F6**).

3.5. Hole M0096E

This hole was cored by wash bore only; no core was recovered (Table **T1**).

3.6. Hole M0096F

A total of 4.48 m of core from Hole M0096F was scanned with the MSCL, and the core exhibited moderate drilling-induced disturbance, resulting in 44% of the acquired data passing QA/QC (see Table **T10** in the Expedition 398 methods chapter [Webster et al., 2025]). Two discrete samples were taken for *P*-wave velocity and MAD measurements. Digital linescans, color reflectance, and hyperspectral imaging were acquired on all cores.

3.6.1. Density and porosity

Density and porosity data are presented in Figures **F8** and **F15** and Table **T2**. MSCL bulk density measurements range 1.37–2.75 g/cm^3. Drilling-induced disturbances and short core lengths compromised the quality of the remaining density data (see **Physical properties** in the Expedition 389 methods chapter [Webster et al., 2025]) and limited sampling. Two discrete samples were analyzed for MAD, giving bulk density values in the range of 2.56–2.70 g/cm^3. Porosity values for the same samples range 17.7%–20.6%, and grain density values fluctuate between 2.956 and 3.067 g/cm^3. There are no clear downhole trends in the density and porosity data sets and no clear relationship between the two bulk density measurements (MSCL and discrete).

3.6.2. *P*-wave velocity

P-wave velocity MSCL measurements yielded no data. Two samples were measured using the discrete *P*-wave logger. Dry measurement values are 3622 and 3908 m/s (Figure **F16**). *P*-wave velocities of 4253 and 4742 m/s were measured for the resaturated samples. Because of the limited *P*-wave data points, there are no apparent downhole trends.

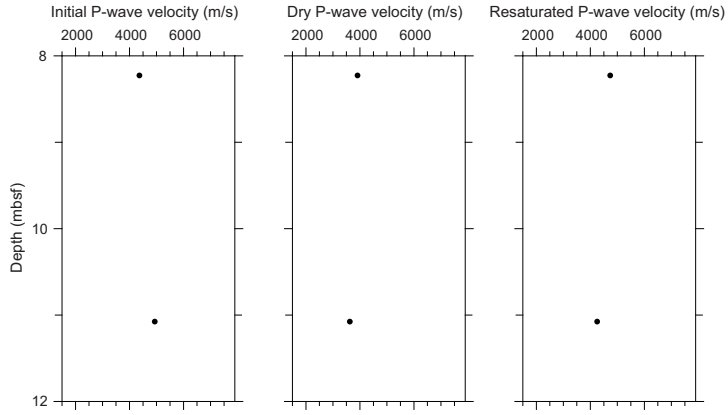

Figure F16. Initial, dry, and resaturated *P*-wave velocities measured on discrete samples, Hole M0096F.

3.6.3. Thermal conductivity

Thermal conductivity was collected on one core (see Table **T11** in the Expedition 398 methods chapter [Webster et al., 2025]) and has a value of 1.533 W/(m·K).

3.6.4. Magnetic susceptibility

MSCL magnetic susceptibility data ranges 72.20 × 10^{-5} to 230.53 × 10^{-5} SI (Figure **F8**) with a mean value close to 127.00 × 10^{-5} SI, values consistent with the lava lithology of the hole.

3.6.5. Electrical resistivity

MSCL noncontact resistivity measurements range 2.11–11.97 Ωm (Figure **F8**). Like the other data sets for this hole, there are no apparent downhole trends, as expected for a hole with rather uniform lithology.

3.6.6. Natural gamma radiation

MSCL NGR measurements display values ranging 26–29 counts/s and show no apparent downhole trend (Figure **F8**).

3.6.7. Digital linescans, color reflectance, and hyperspectral imaging

All cores were digitally scanned, and, where appropriate, measured for color reflectance and imaged with the hyperspectral scanner (see HYPERSPECTRAL in **Supplementary material**). Color reflectance L* values vary between 13.05% and 34.68%, a* varies between –1.00 and 2.76, b* varies between –0.65 and 12.25, and a*/b* varies between –0.59 and 0.31 (Figure **F8**).

4. Geochemistry

4.1. Interstitial water

No interstitial water samples were collected from Site M0096.

4.2. Surface seawater

A surface seawater sample was collected from Site M0096 using an improvised sampling device from the side of the vessel (see Figure **F22** in the Expedition 389 methods chapter [Webster et al., 2025]). The salinity, pH, alkalinity, ammonium, and major element chemistry measured for this sample are consistent with the other surface seawater samples taken during Expedition 389 and align with the expected values for conservative elements in seawater (see Tables **T15** and **T17** in the Expedition 389 methods chapter [Webster et al., 2025]).

4.3. Bulk sediment and rocks

A total of three lava samples were taken from Site M0096 (Figure **F2**) and analyzed for mineralogy, elemental composition, and carbon content. Sample 389-M0096F-4R-1, 16–17.5 cm (9.83 mbsf), was taken from a section of visually altered lava, whereas samples from Holes M0096A and M0096D were from smaller pieces of visually fresh lava.

4.4. Mineralogy

XRD analyses for Site M0096 are presented in Table **T3**. The mineralogy of Sample 389-M0096F-4R-1, 16–17.5 cm (9.83 mbsf), indicates moderately altered basalt, containing 48% secondary carbonate minerals (high-Mg calcite [29%] and mixed carbonates [19%]) and roughly 40% primary igneous minerals. The igneous components consist of a nearly equal abundance of high-Ca (anorthic) plagioclase feldspar (21%) and Mg-Ca (diopsan) clinopyroxene. Additionally, this specimen includes detectable clinoptilolite (zeolite; 4%) and cristobalite (5%), consistent with elevated temperatures during aqueous alteration. Visual inspection of the specimen indicates secondary carbonate is present as void infilling, rather than igneous mineral replacement (i.e., alteration). The

Table T3. HighScore XRD mineral abundances, Site M0096. **Download table in CSV format.**

Table T4. Solid-phase elemental abundances, Site M0096. **Download table in CSV format.**

Table T5. TOC, TIC, and TC, Site M0096. **Download table in CSV format.**

specimen also contains volumetrically minor quantities of cristobalite (a high-temperature silica polymorph; 5%) and montmorillonite clay.

Sample 389-M0096A-1R-1, 24–27 cm (0.24 mbsf), consists of a mix of plagioclase (43%) and pyroxenes (22%) with some Mg-rich calcite (24%) and aragonite (7%) likely resulting from contamination from bioclasts. Lava rock Sample 389-M0096D-3R-1, 0–2 cm (4.56 mbsf), contains 99% pyroxene.

4.5. Elemental abundances

The concentrations of major elements in the lava rock samples from Site M0096 (Table **T4**) reflect the alteration and heterogeneity of the sample. Sample 389-M0096F-4R-1, 16–17.5 cm (9.83 mbsf), has higher Ca, Ti, and Zr, consistent with alteration products in the sample. This was also evident in the XRD data and visual inspection. Sample 389-M0096D-03R-1, 0-2 cm (4.56 mbsf), exhibits higher Mg, Cr, and Ni.

4.6. Carbon content

The results for total organic carbon (TOC), total carbon (TC), and total inorganic carbon (TIC) for the three samples measured at Site M0096 are presented in Table **T5**. The TOC content ranges 0.10%–0.16%, and the TIC content ranges 0.7%–3.0% (calculated to be 6%–25% $CaCO_3$; see GEOCHEM in **Supplementary material**). Sample 389-M0096F-4R-1, 16–17.5 cm (9.83 mbsf), has a slightly higher organic carbon content than the other volcanic samples from Site M0096.

5. Paleomagnetism

A total of eight plug samples were obtained from Holes M0096A, M0096D, and M0096F. Measurements of low-field and mass-specific magnetic susceptibility (χ) were carried out for all samples. The initial natural remanent magnetization (NRM) was measured for all samples, as was remanence following stepwise alternating field demagnetization up to maximum applied fields of 100 mT (Table **T6**). For further details, see **Paleomagnetism** in the Expedition 389 methods chapter (Webster et al., 2025).

5.1. Hole M0096A

One sample was taken from Hole M0096A (Sample 1R-1, 29–31 cm). It is primarily composed of lava. The low-field and mass-specific χ of the sample is 5.16×10^{-6} m^3/kg. The initial NRM intensity is 1.28 A/m.

5.2. Hole M0096B

This hole was cored by wash bore only; no core was recovered (Table **T1**).

5.3. Hole M0096C

No samples for paleomagnetic analyses were taken from Hole M0096C.

5.4. Hole M0096D

Two samples were obtained from Hole M0096D. One is composed of carbonate (Sample 3R-1, 48–50 cm) and the other lava (Sample 3R-2, 23.5–26.5 cm). The carbonate sample shows a negative χ value of -1.66×10^{-9} m^3/kg and a low initial NRM intensity of 4.50×10^{-3} A/m. In contrast, the lava sample shows a strong positive χ value of 4.28×10^{-5} m^3/kg and a high initial NRM intensity of 1.94×10^{1} A/m.

Table T6. Magnetic susceptibility and NRM, Holes M0096A and M0096D. **Download table in CSV format.**

Core, section, interval (cm)	Sample type	Depth (mbsf)	Magnetic susceptibility (m^3/kg)	Initial NRM intensity (A/m)
389-M0096A-				
1R-1, 29–31	Basalt	0.30	5.16×10^{-6}	1.28
389-M0096D-				
3R-1, 48–50	Carbonate	5.05	-1.66×10^{-9}	4.50×10^{-3}
3R-2, 23.5–26.5	Basalt	5.34	4.28×10^{-5}	1.94×10^{1}

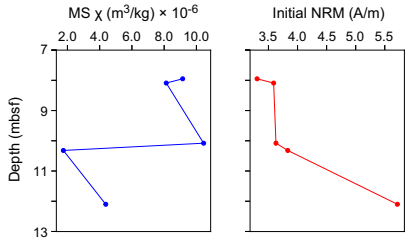

Figure F17. Magnetic susceptibility (MS) and NRM, Hole M0096F.

5.5. Hole M0096E

This hole was cored by wash bore only; no core was recovered (Table **T1**).

5.6. Hole M0096F

Five lava samples were collected from Hole M0096F. High positive χ values are observed throughout the hole, ranging 1.75×10^{-6} to 10.4×10^{-6} m^3/kg. The initial NRM intensities decrease from 5.72 A/m at the bottom of the hole to 3.30 A/m at the top (Figure **F17**).

6. Geochronology

One U-Th date was obtained from a coral near the top of Hole M0096D (Sample 3R-1, 45–47 cm); it was not rejected (see Tables **T21** and **T22** in the Expedition 389 methods chapter [Webster et al., 2025]). The date is consistent with the interpretation of the age of this H4 terrace from previous studies (Ludwig et al., 1991; Webster et al., 2009).

References

Ludwig, K.R., Szabo, B.J., Moore, J.G., and Simmons, K.R., 1991. Crustal subsidence rate off Hawaii determined from $^{234}U/^{238}U$ ages of drowned coral reefs. Geology, 19(2):171–174. **https://doi.org/10.1130/0091-7613(1991)019<0171:CSROHD>2.3.CO;2**

Webster, J.M., Braga, J.C., Clague, D.A., Gallup, C., Hein, J.R., Potts, D.C., Renema, W., Riding, R., Riker-Coleman, K., Silver, E., and Wallace, L.M., 2009. Coral reef evolution on rapidly subsiding margins. Global and Planetary Change, 66(1–2):129–148. **https://doi.org/10.1016/j.gloplacha.2008.07.010**

Webster, J.M., Ravelo, A.C., Grant, H.L.J., and the Expedition 389 Scientists, 2025. Supplementary material, **https://doi.org/10.14379/iodp.proc.389supp.2025.** In Webster, J.M., Ravelo, A.C., Grant, H.L.J., and the Expedition 389 Scientists, Hawaiian Drowned Reefs. Proceedings of the International Ocean Discovery Program, 389: College Station, TX (International Ocean Discovery Program).

Webster, J.M., Ravelo, A.C., Grant, H.L.J., Rydzy, M., Stewart, M., Allison, N., Asami, R., Boston, B., Braga, J.C., Brenner, L., Chen, X., Chutcharavan, P., Dutton, A., Felis, T., Fukuyo, N., Gischler, E., Greve, S., Hagen, A., Hamon, Y., Hathorne, E., Humblet, M., Jorry, S., Khanna, P., Le Ber, E., McGregor, H., Mortlock, R., Nohl, T., Potts, D., Prohaska, A., Prouty, N., Renema, W., Rubin, K.H., Westphal, H., and Yokoyama, Y., 2025. Expedition 389 methods. In Webster, J.M., Ravelo, A.C., Grant, H.L.J., and the Expedition 389 Scientists, Hawaiian Drowned Reefs. Proceedings of the International Ocean Discovery Program, 389: College Station, TX (International Ocean Discovery Program). **https://doi.org/10.14379/iodp.proc.389.102.2025**